ADVANCED MATERIALS
www.advmat.de

Universal Stripe Symmetry of Short-Range Charge Density Waves in Cuprate Superconductors

Jaewon Choi, Jiemin Li, Abhishek Nag, Jonathan Pelliciari, Hannah Robarts, Charles C. Tam, Andrew Walters, Stefano Agrestini, Mirian García-Fernández, Dongjoon Song, Hiroshi Eisaki, Steve Johnston, Riccardo Comin, Hong Ding, and Ke-Jin Zhou**

The omnipresence of charge density waves (CDWs) across almost all cuprate families underpins a common organizing principle. However, a longstanding debate of whether its spatial symmetry is stripe or checkerboard remains unresolved. While CDWs in lanthanum- and yttrium-based cuprates possess a stripe symmetry, distinguishing these two scenarios is challenging for the short-range CDW in bismuth-based cuprates. Here, high-resolution resonant inelastic x-ray scattering is employed to uncover the spatial symmetry of the CDW in $Bi_2Sr_{2-x}La_xCuO_{6+\delta}$. Across a wide range of doping and temperature, anisotropic CDW peaks with elliptical shapes are found in reciprocal space. Based on Fourier transform analysis of real-space models, the results are interpreted as evidence of unidirectional charge stripes, hosted by mutually 90°-rotated anisotropic domains. This work paves the way for a unified symmetry and microscopic description of CDW order in cuprates.

1. Introduction

Symmetry is a fundamental language to describe the nature of materials. Identifying the symmetry of ordered states is the first stepping stone to understanding their properties. However, it is often challenging to unambiguously unveil the symmetry of "quantum materials" due to interplay among different ordered states and material-related complications such as disorder. High-temperature copper-oxide (or "cuprate") superconductors (SCs) are prime examples of such quantum materials that exhibit a unique set of broken-symmetry phenomena,[1,2] such as pseudogap,[3–6] strange metal behavior,[7–9]

J. Choi, J. Li, A. Nag, H. Robarts, C. C. Tam, A. Walters, S. Agrestini, M. García-Fernández, K.-J. Zhou
Diamond Light Source
Harwell Campus
Didcot, Oxfordshire OX11 0DE, UK
E-mail: jaewon.choi@diamond.ac.uk; kejin.zhou@diamond.ac.uk

J. Li, H. Ding
Beijing National Laboratory for Condensed Matter Physics and Institute of Physics
Chinese Academy of Science
Beijing 100190, China

J. Pelliciari, R. Comin
Department of Physics
Massachusetts Institute of Technology
Cambridge, MA 02139, USA

J. Pelliciari
National Synchrotron Light Source II
Brookhaven National Laboratory
Upton, NY 11973, USA

H. Robarts, C. C. Tam
H. H. Wills Physics Laboratory
University of Bristol
Bristol BS8 1TL, UK

D. Song, H. Eisaki
National Institute of Advanced Industrial Science and Technology (AIST)
Tsukuba, Ibaraki 305-8560, Japan

D. Song
Stewart Blusson Quantum Matter Institute
University of British Columbia
Vancouver BC V6T 1Z4, Canada

S. Johnston
Department of Physics and Astronomy
The University of Tennessee
Knoxville, TN 37996, USA

S. Johnston
Institute for Advanced Materials and Manufacturing
The University of Tennessee
Knoxville, TN 37996, USA

H. Ding
Tsung-Dao Lee Institute & School of Physics and Astronomy
Shanghai Jiao Tong University
Shanghai 200240, China

H. Ding
CAS Center for Excellence in Topological Quantum Computation
University of Chinese Academy of Sciences
Beijing 100190, China

The ORCID identification number(s) for the author(s) of this article can be found under https://doi.org/10.1002/adma.202307515

DOI: 10.1002/adma.202307515

nematicity,[10–13] and various density-wave states.[14–21] Among these, charge-density waves (CDWs) — periodic modulations of valence electron density — have been ubiquitously discovered in both hole- and electron-doped cuprates.[14–32] This universality has prompted suggestions of a unified principle underlying their formation, and thus may hold a key to solve the enigma of high-temperature superconductivity and complex phase diagram of cuprates.

However, there has been a longstanding controversy, that is, whether the spatial symmetry of the CDW ordered state, *i.e.*, ~~the~~its microscopic structure, is bidirectional "checkerboard" or unidirectional "stripe".[33] Although the presence of intertwined spin-charge stripe order is widely perceived, especially in lanthanum (La)-based cuprates,[15] the formation of mutually 90°-rotated charge stripe domains due to two equivalent Cu-O bond directions in the square-lattice CuO_2 plane leads to experimental results virtually indistinguishable from those of checkerboard CDW. For example, both CDW symmetries commonly generate fourfold electronic diffraction peaks along *H* and *K* directions in reciprocal space.[34,35]

There have been a number of theoretical and experimental works to resolve the above debate in three major categories of hole-doped cuprate superconductors: La-, yttrium (Y)- and bismuth (Bi)-based materials. Recent x-ray scattering experiments on La-based[36,37] and Y-based cuprates[38,39] overcame this challenge by taking the strategy of employing an uniaxial pressure as an external symmetry-breaking perturbation to lift the degeneracy of two symmetry candidates, and successfully revealed a unidirectional nature of the CDW. For Bi-based compounds that exhibit a higher SC transition temperature T_c above 90 K, however, uniaxial pressure is hardly applicable due to the fragility of thin crystals. Thus, alternative strategies have been considered. For example, a plethora of scanning tunnelling microscopy (STM) studies reported a short-range checkerboard-like electronic modulation along Cu-O bond directions in real space with a four-unit-cell periodicity.[18,24–29] Interestingly, recent STM works revealed unidirectional nano-clusters of electronic modulation with *d*-wave form factor in double-layer $Bi_2Sr_{2-x}Ca_xCu_2O_{8+\delta}$ (Bi2212).[40–44] However, the unidirectional nature is less evident in recent STM and scattering experiments on single-layer $Bi_2Sr_{2-x}La_xCuO_{6+\delta}$ (La-Bi2201).[28,29,35]

Elucidating the CDW symmetry in Bi-based cuprates will therefore be indispensable for answering the question: is the unidirectional "stripe" CDW symmetry universal for all cuprate materials? Since the CDW is intimately related with superconductivity, this question may be essential for understanding the interplay of CDW, SC, and other broken-symmetry states. For example, there have been a number of theoretical works suggesting that the fluctuating stripe may play a significant role in the mechanism of SC.[45–49] In addition, a unidirectional pair-density-wave order (PDW), where a SC order parameter is intertwined with CDW and periodically modulated, has been proposed as a "primary" order in cuprates.[50] The exact answer to the question of CDW spatial symmetry is pivotal to differentiate microscopic models of PDW order parameter.[51]

To address this question, we performed high-resolution resonant inelastic x-ray scattering (RIXS) measurements on $Bi_2Sr_{2-x}La_xCuO_{6+\delta}$ (La-Bi2201). Instead of applying uniaxial pressure, we developed mapping the CDW patterns in (*H*, *K*) 2D reciprocal space to extract the information about its microscopic structure in real space. Although there have been several RIXS studies on the CDW order in Bi-based cuprates,[52–55] they only focus along the primary (*H*, 0) or (0, *K*) direction. Our work is the first systematic investigation of the CDW symmetry by expanding the capability of the RIXS technique into 2D reciprocal space mapping. Energy-resolved high-resolution RIXS has the advantage of disentangling weak quasielastic short-range CDW responses from the phonon modes as well as the spin and *d*-*d* orbital excitations, and therefore, ideal for the exploration of CDW symmetry in Bi-based cuprates.[30] In addition, RIXS is complementary to surface-probing techniques such as STM, as it is more sensitive to bulk information in macroscopic length scale. Our systematic RIXS mapping studies reveal that the CDW patterns in La-Bi2201 possess an elliptical shape, elongated along the transverse direction. This anisotropic CDW pattern was robustly found in a wide range of temperatures and doping concentrations. By Fourier-transform analysis of real-space models, we concluded that equally populated 90°-rotated domains of charge stripe orders lead to anisotropic CDW peaks. This result implies that the unidirectional stripe symmetry may be a generic property of CDWs in cuprate material families.

2. Results and Discussion

The CDW order in La-Bi2201 system manifests itself as quasielastic scattering intensity peaks at four symmetry-equivalent positions in reciprocal space, $(H, K) = (\pm\delta, 0)$ and $(0, \pm\delta)$, where the incommensurability $1/5 < \delta < 1/3$ reciprocal lattice unit (r.l.u.) is consistent with previous reports.[27,54] By applying a complex rotation algorithm with respect to the CDW peak, we obtained momentum-dependent RIXS spectra across the CDW peaks at $(\delta, 0)$ and $(0, \delta)$, hereafter denoted as *H*- and *K*-CDW, with different scan angle α as illustrated in **Figure 1a**. Here, α is defined as the angle between the actual scan and the longitudinal propagating direction. The incoming photon energy was tuned to the resonances of Cu L_3-edge (≈931.6 eV) and O *K*-edge (≈528.4 eV) absorption energy to maximize the sensitivity to CDW (Figure 1b,c). An enhancement in the quasielastic scattering intensity integrated over the energy window of ±25 meV is clearly identified in underdoped La-Bi2201 ($x = 0.6$, $T_c = 23$ K, UD23K) near $\mathbf{Q} = (0.25, 0)$ and $(0, 0.25)$ at both Cu and O sites, confirming a multiorbital nature of the CDW[54] (Figure 1d,e).

To gain an overview of CDW patterns, we show representative CDW scans obtained at Cu L_3-edge at selected values of α across *H*-CDW (Figure 1f) and *K*-CDW (Figure 1g) of the UD23K sample. The full-width half-maximum (FWHM) of *H*-CDW in the transverse direction ($\alpha = 90°$) is noticeably larger than that in the longitudinal direction ($\alpha = 0°$), demonstrating an anisotropic CDW peak structure. Examination of *K*-CDW reveals the same anisotropy with comparable FWHMs. We also found the elongated CDWs present along both *H* and *K* directions at O *K*-edge (see Figure S3, Supporting Information).

We now scrutinize the analysis on the shape of the individual CDW peaks. Figure 1h summarizes the extracted FWHM of *H*-CDW and *K*-CDW at both Cu L_3- and O *K*-edges in La-Bi2201 UD23K as a function of α from -97.5° to 150° (Figures S2 and S3, Supporting Information). Clearly the data show an

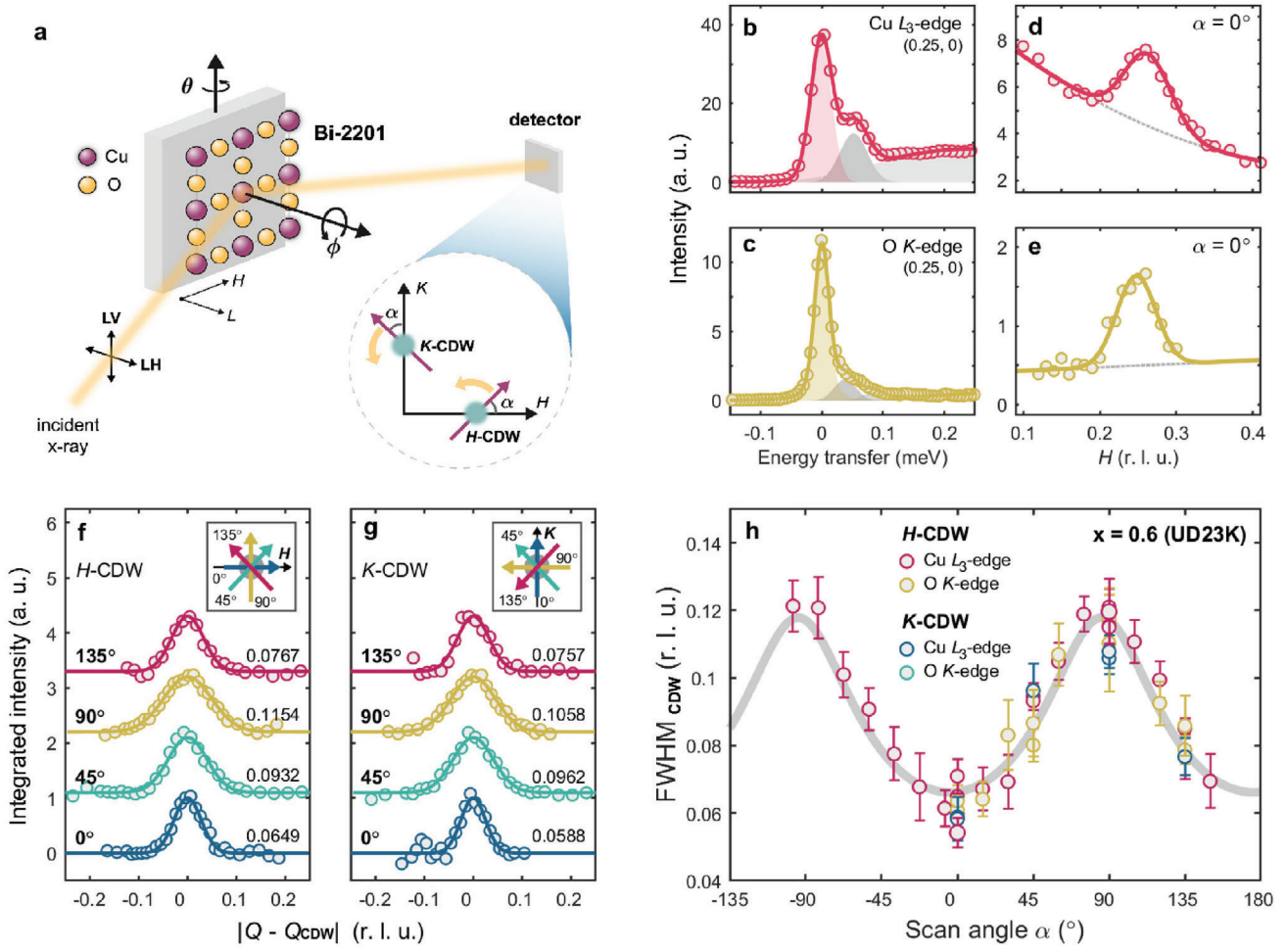

Figure 1. Angular-dependent RIXS experiment on charge-density wave (CDW) in La-Bi2201. a), Schematic illustration of the RIXS experiment. By changing an in-plane sample rotation ϕ, *H*- and *K*-CDWs are sliced along different directions, defined by scan angle α, in the (*H*, *K*) plane. b,c) Representative RIXS spectra at Q = (0.25, 0) with Cu L_3 (b) and O *K* resonance (c) obtained from La-Bi2201 $x = 0.6$ (UD23K). Spectral weight from quasielastic, phonon, and paramagnon contribution is highlighted by red (or cyan for O K-edge), dark-grey, and light-grey color, respectively. d,e) CDW peaks extracted from RIXS spectra as a function of *H* at Cu L_3- and O *K*-edge. Solid lines are Gaussian fits with polynomial background. f,g) Background-subtracted momentum-dependent CDW profiles of integrated intensity across the wavevector of *H*-CDW (f) and *K*-CDW (g) at Cu L_3-edge with different scan angle α. The insets depict scan directions. The number on the right side of each profile corresponds to fitted full-width half-maximum (FWHM). h) FWHMs of *H*- and *K*-CDW peaks measured at both absorption edges are plotted as a function of α. The grey solid line indicates the least square fit to elliptical equation (See Methods). All data were obtained from La-Bi2201 $x = 0.6$ (UD23K) at $T = 23$ K.

oscillatory behavior as a function of α. The least square fit of the data to an elliptical equation (the grey solid line in Figure 1h, Methods) returns the maximum ≈0.118 r.l.u. near $\alpha = 90°$ and the minimum ≈0.066 r.l.u. near $\alpha = 0°$. The major and minor axes along 0° and 90° indicate that the CDW propagation is locked along two orthogonal Cu-O bond directions. The aspect ratio of 1.8 implies the CDW correlation, *i.e.*, $\xi = 2/\text{FWHM}$, in the longitudinal direction ($\xi_{\parallel}$ ≈18.7 Å) is almost twice as long as that in the transverse direction ($\xi_{\perp}$ ≈10.4 Å). In **Figure** 2c,d, the same set of data are plotted in polar coordinates. The shape of the individual CDW peak is best described as an ellipse elongated along the transverse direction, perpendicular to the direction of CDW propagation. The *K*-CDW ellipse possesses almost the same size but is rotated by 90°, implying that the CDW pattern in reciprocal space preserves fourfold (C_4) symmetry, seemingly reflecting the nature of the underlying CuO_2 square-lattice.

We extended the same RIXS study to explore the doping and temperature dependence. Our primary motivation is to investigate whether the anisotropic CDW peak is universally present in a broad region of the phase diagram. Figure 2a,b,e,f exhibit the CDW peaks obtained from a non-superconducting ($x = 0.8$, $T_c = 30$ K, non-SC) and an optimally-doped ($x = 0.4$, OD30K) La-Bi2201, respectively. Figure 2g summarizes the longitudinal correlation length, $\xi_{\parallel}$, and the transverse correlation length, $\xi_{\perp}$, of the samples with different hole doping concentration *p*. $\xi_{\parallel}(p)$ reaches its maximum at $p \approx 0.13$ (UD23K) whereas $\xi_{\perp}(p)$ shows a monotonically decreasing trend. Here, we introduce the ratio $\eta = \xi_{\perp}/\xi_{\parallel}$ to represent the degree of anisotropy in the width of CDW peaks. For all three doping concentrations, the CDW peak

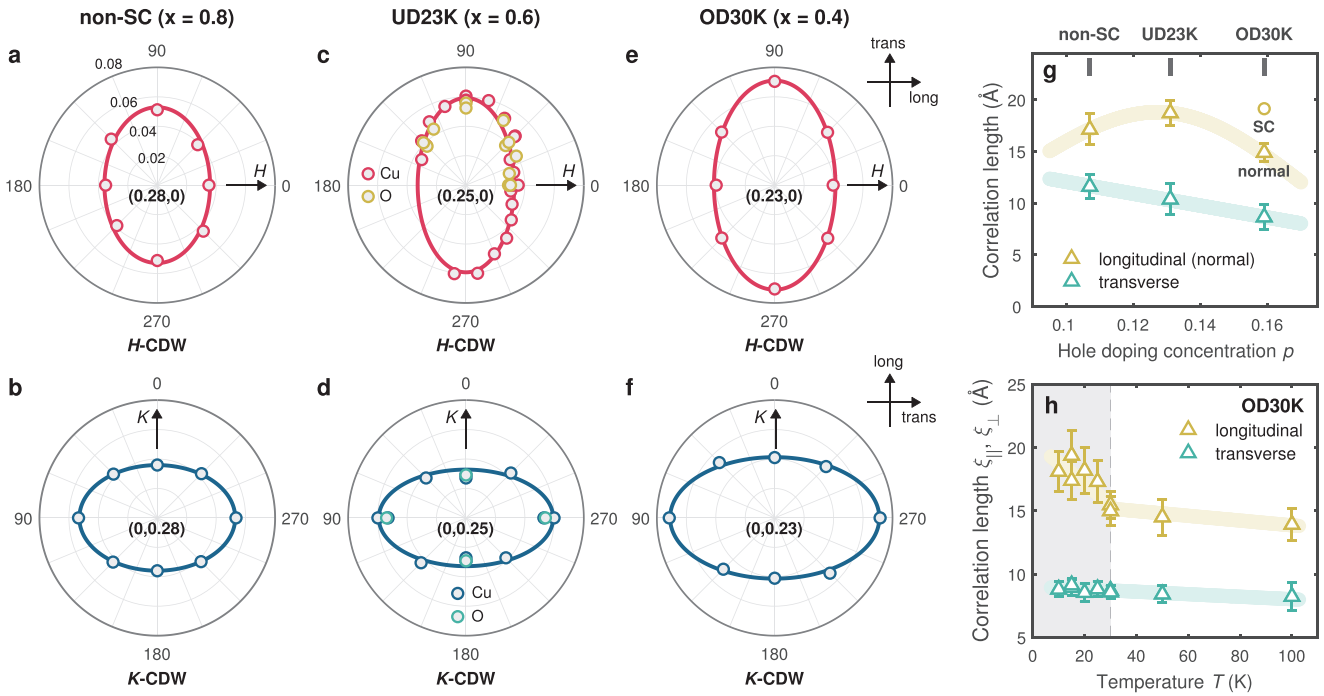

Figure 2. Doping and temperature evolution of anisotropic CDW correlation. a--f) Full-width half-maximum of both *H*-CDW (upper panels) and *K*-CDW (lower panels) peaks in La-Bi2201 with different doping concentrations as stated. Solid lines are least-square fits to elliptical equations (see Methods). Arrows on the upper right corner depict longitudinal (long) and transverse (trans) scan directions across each CDW. g,h) Hole doping concentration p (g) and temperature T dependence (h) of longitudinal and transverse CDW correlations. The data presented by open triangles in (g) are measured at temperatures inside the normal phase or close to the normal-SC phase boundary (20, 23, and 30 K for non-SC, UD23K, and OD30K, respectively), except for the open circle measured inside of the SC phase. The grey dashed line in (h) indicates the superconducting transition temperature T_c. The colored trends are guided to the eye.

has an anisotropic shape ($\eta > 1$). Temperature studies revealed that $\xi_{\parallel}$ is always greater than $\xi_{\perp}$ in OD30K sample (Figure 2h). As a result, the ratio η stays to be larger than 1.5 up to $T \approx 100$ K (see Figure S4a, Supporting Information), confirming the robust existence of the anisotropic CDW peaks in a wide range of temperatures. We also observed an interesting behavior: $\xi_{\parallel}$ increases much faster below T_c, whereas $\xi_{\perp}$ displays a continuous linear trend. As a result, η starts to increase inside the SC phase and reaches almost two at the lowest temperature $T = 10$ K. Its implications will be discussed at the end of the section.

The CDW peak patterns in reciprocal space probed by RIXS encode the spatial symmetry of the CDW order in real space. We thus performed theoretical simulations by constructing idealized models, that is, the real-space electronic modulation with either stripe or checkerboard pattern, where both anisotropic and isotropic domains are considered. For each scenario, two individual CDW domains are included with a 90° rotation from each other to mimic the equally populated orthogonal domains (insets of **Figure** 3a–d, and see Supporting Information). The real-space electron density modulation maps $\rho(x, y)$ were built by translating the orthogonal CDW domains in the x and y directions with a random phase shift to represent the actual samples probed by RIXS (Figure 3a–d). Fourier transforms of the electron density maps $\rho(x, y)$ yield a unique CDW reciprocal-space pattern for each scenario (Figure 3e–h). For instance, an anisotropic stripe symmetry produces elliptical CDW diffraction peaks, preserving the C_4 symmetry but elongated in the transverse direction (Figure 3e). The anisotropic checkerboard domains give rise to star-shaped CDW peaks elongated along both the transverse and longitudinal directions (Figure 3f). On the other hand, isotropic checkerboard and isotropic stripe phases generate virtually indistinguishable isotropic CDW peaks (Figure 3g,h). Remarkably, our experimental observations in La-Bi2201 (Figure 2) coincide with the spatial symmetry of CDW order having unidirectional stripe, rather than bidirectional checkerboard. A consistent conclusion is achieved based on similar Fourier transform analysis on more realistic electron density maps (Figure S7, Supporting Information).[56]

At the first glance, it may look perplexing that we straightforwardly obtain the unambiguous agreement between experiment and theoretical modeling, while the CDW symmetry had been debated in a considerable number of earlier STM studies.[18,19,24–26,28,29] The static checkerboard-like modulation was proposed for Bi-based cuprates from tunneling electron conductance maps. In their Fourier-transformed images, fourfold symmetry-equivalent peaks typically appear at an incommensurate wavevector position.[18,24–29] However, the conservation of C_4 symmetry is not a unique signature of the checkerboard-like modulation pattern as the coexistence of orthogonal domains of unidirectional stripe-like CDW also produces a fourfold peak pattern. More sophisticated analysis on the tunneling asymmetry at the pseudogap energy scale reveals the presence of four-unit-cell-wide unidirectional nanodomains[40–42] with predominant *d*-wave form factor breaking C_4 rotational symmetry by differing the phase between O_x and O_y orbitals in the CuO_2 layer by π.[43,44]

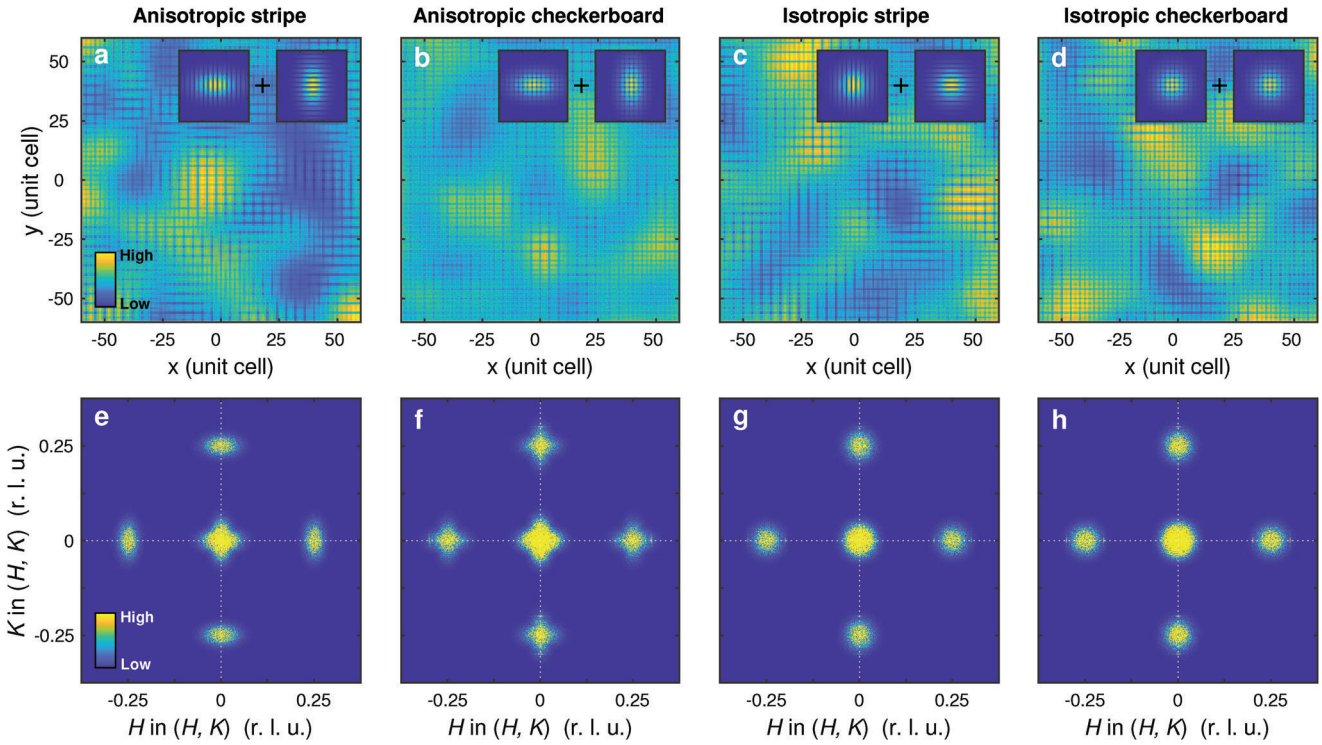

Figure 3. Model CDW modulation in real and reciprocal space. a–d), Real-space electron density modulation map $\rho(x, y)$ calculated by assuming equal population of a) anisotropic 90°-rotated stripe domains, b) 90°-rotated anisotropic checkerboard domains, c) 90°-rotated isotropic stripe domains, and d) isotropic checkerboard domains. e–h), Corresponding CDW peak patterns in reciprocal space, obtained by direct Fourier transformation of (a–d), respectively.

This observation can be interpreted as a fluctuating "stripe" with a short correlation. It is worth noting that the nature of short-range CDW order imposes severe challenges on the assessment of the symmetry based on real-space images, which manifest visually checkerboard-like CDW patterns regardless of whether its intrinsic symmetry is stripe or checkerboard, as shown by our modeled density maps (Figure 3a–d) as well as advanced theoretical studies.[57] For the single-layer La-Bi2201, STM has not yet provided conclusive evidence for stripe symmetry of CDW order.[25,28,29,58] Thus, our results show that energy-resolved RIXS is an efficient experimental probe of microscopic structure of CDW-ordered ground state in disordered systems with short correlation length.

In this sense, we have demonstrated that RIXS is a complementary technique as it is more sensitive to the property of bulk materials in macroscopic length scale and it probes CDW spatial symmetry directly in reciprocal space. Establishing the link between x-ray scattering and STM techniques, which probes reciprocal and real space, respectively, is among the most important and challenging tasks. Besides the presence of electronic modulation with a four-unit-cell periodicity, we make a clear correspondence between the two techniques by confirming the unidirectional nature of CDW in Bi-based cuprate material families. This correspondence was further strengthened by the recent high-resolution STM observation of electron-lattice coupling in the pseudogap region of Bi2212.[59] It visualizes the local lattice distortion with four-unit-cell periodicity breaking fourfold rotational symmetry, similar to the anomalies in bond-stretching phonon revealed by RIXS experiments.[54,55]

Elongated CDW peaks in reciprocal space were also found in Y-based cuprates by resonant elastic x-ray scattering (REXS) and proposed as evidence of unidirectional stripe-like CDW order.[34] The interpretation was challenged as the corresponding real-space correlation function $C(x, y)$, *i.e.*, the direct Fourier transform of the reciprocal-space CDW pattern similar to Figure 3e, appears checkerboard-like.[56] The calculation of $C(x, y)$ via autocorrelation of the real-space electron density maps (Figure 3a–d) confirmed all four scenarios induce comparable checkerboard-like patterns akin to previous reports (Figure S6, Supporting Information).[56] Therefore, it is challenging to directly visualize the symmetry of a short-range CDW from either the electron density map $\rho(x, y)$ or correlation function $C(x, y)$ in real space. Instead of examining the shape of CDW peaks, a recent RIXS study under uniaxial pressure reveals a unidirectional nature of CDW in Y-based cuprates.[39] The anisotropic CDW peaks we observed in La-Bi2201 are in stark contrast to isotropic CDW peaks reported in La-based[60–63] and Hg-based cuprate materials.[64] For $La_{1.88}Sr_{0.12}CuO_4$, twinned domains of slanted stripe order with ±3° away from Cu-O bond directions result in two CDW peaks along transverse direction, eventually merging into a single isotropic peak under mild uniaxial pressure.[63] Despite the isotropic peak shape, x-ray diffraction employing uniaxial pressure unambiguously verifies charge stripe order.[36]

Before we conclude, it is worth emphasizing that the response of CDW correlation $\xi_{\parallel}$ and $\xi_{\perp}$ is not isotropic upon the change

in doping and temperature (Figure 2g,h). For example, $\xi_{\perp}$ monotonically decreases as a function of p, whereas $\xi_{\parallel}$ is maximized at $p \approx 0.13$ (UD23K sample). As a result, the ratio η, which can be interpreted as an order parameter for "stripeness", is maximized at p close to the so-called 1/8 magical doping concentration that the CDW possesses its largest onset temperature in virtually all cuprate material families.[33] Furthermore, the CDW wavevector in this sample is ≈0.25 r.l.u, close to being commensurate with four-unit-cell periodicity. We speculate that the system shows susceptibility toward a stripe order when the CDW approaches to be commensurate with the underlying CuO_2 lattice due to the dynamical pinning effect.

The enhancement of $\xi_{\parallel}$ below T_c, coincided with the same trend in the CDW peak intensity (Figure S4a, Supporting Information), may suggest "cooperative" interplay between the stripe short-range CDW and SC orders. As short-range CDW is not weakened inside the SC phase in several other cuprates,[27,30,65] the relationship between two orders can be understood by cooperation, rather than a simple competition picture.[21,36,66,67] It is also interesting that $\xi_{\parallel}$ is not affected by temperature, so "stripeness" also increases inside the SC phase (Figure S4b, Supporting Information). This indicates that the "cooperative" interplay is unidirectional and two orders are coupled to form a composite order parameter. Thus, optimally-doped La-Bi2201 may be a good candidate for a pair-density-wave (PDW) state,[51] where the SC order parameter is unidirectionally modulated due to the interplay with CDW, proposed as "stripe" superconductivity[68,69] that has experimentally been observed in Bi2212.[44,70] A recent STM work identified a checkerboard domain pattern with internally unidirectional periodic modulation of SC gap,[71] consistent with our interpretation.

3. Conclusion

We have investigated the spatial symmetry of short-range CDWs in the Bi-based cuprate superconductor La-Bi2201 by employing a high-resolution RIXS technique. By mapping out the reciprocal space, the fourfold CDW peaks with an anisotropic shape, elongated along the transverse direction, are robustly present in a broad range of temperatures and doping concentrations. Fourier-transform analysis based on the reconstructed real-space map confirms that the anisotropic CDW peaks can be attributed to the presence of 90°-rotated short-range charge stripe domains. Alongside the results from La- and Y-based cuprates, our study corroborates unidirectional stripes as the fundamental symmetry of CDWs across different cuprate materials. This remarkable universality not only provides a perspective on the unified organizing principle of CDW and its role in cuprate phase diagram, but also constrains the symmetry in microscopic models describing CDW and the interplay with other ordered phases.

4. Experimental Section

Sample Growth and Characterization: High-quality single crystals of $Bi_2Sr_{2-x}La_xCuO_{6+\delta}$ (La-Bi2201) with La doping concentrations of x = 0.8 (non-SC), x = 0.6 (T_c = 23 K, UD23K), x = 0.4 (T_c = 30 K, OD30K) were synthesized by the traveling-solvent floating-zone method. The hole doping concentration p was calculated by the empirical linear relation between x and p: $p = 0.21 - 0.128x$.[72] The as-grown samples were annealed at 650°C in an oxygen atmosphere for two days to improve the homogeneity of the samples. The sample orientation was characterized by Laue diffraction prior our resonant x-ray inelastic scattering (RIXS) experiments. Superstructure reflections propagating along Cu-Cu bond direction, or equivalently along (H, H) direction, were identified by the Laue diffraction method. All samples were cleaved by mechanical exfoliation, before transferring to a loadlock chamber.

X-ray Absorption Spectroscopy: X-ray absorption spectra of La-Bi2201 samples were collected with a normal incidence geometry ($\theta = 90°$) prior to the RIXS experiments. The total electron yield method was employed by measuring the drain current from the samples. Figure S1a,b (Supporting Information) show representative x-ray absorption spectra of La-Bi2201 x = 0.6 (UD23K) near Cu L_3 and O K absorption edges, respectively. The data exhibit a single resonance peak at an energy of 931.6 and 528.4 eV.

High-Resolution RIXS Experiments: High-resolution RIXS experiments on La-Bi2201 were performed at the I21 RIXS beamline of Diamond Light Source in the United Kingdom.[73] The experimental geometry is schematically illustrated in Figure 1a of the main text. Samples were glued on the holder such that its surface normal was the crystallographic c-axis direction. A wavevector $\mathbf{Q}$ was defined by employing pseudo-tetragonal notation $\mathbf{Q} = H\mathbf{a}^* + K\mathbf{b}^* + L\mathbf{c}^*$, or equivalently, $\mathbf{Q} = (H, K, L)$ where $a^* = 2\pi/a$, $b^* = 2\pi/b$, $c^* = 2\pi/c$ are the reciprocal lattice unit vectors and H, K, L are the indices in reciprocal space spanned by a^*, b^*, and c^*. The lattice parameters of La-Bi2201 are $a = b = 3.86$ Å and $c = 24.69$ Å. The incoming x-rays were tuned to the resonant energy of Cu L_3 and O K-edge to maximize the signal sensitivity to CDW residing in the CuO_2 plane. Linear vertical, or σ polarization was used throughout the measurements. The outgoing x-rays emitted from the La-Bi2201 sample pass through paraboloidal collecting optics with a large horizontal acceptance angle inside the main sample chamber to enhance the x-ray photon throughput. The spherical grating optics implemented on a spectrometer to vertically monochromatize emitted x-rays and focus on an area detector. The energy resolution of 37.0 and 27.3 meV was achieved for Cu L_3- and O K-edge, respectively. The scattering angle 2θ was fixed to 154°.

RIXS Data Fitting: RIXS spectra were first normalized to the incident photon flux and the spectral weight of dd excitation integrated over an energy range of 1.2–3 eV. The position of the quasi-elastic peak, or zero-energy position, was determined by measuring the amorphous carbon sample. Compared to energy-integrated resonant elastic x-ray scattering (REXS), the energy-resolved RIXS has the advantage of filtering out unwanted contributions from inelastic scatterings due to various low-energy excitations such as phonon, magnon, and orbital (dd) excitations. To better disentangle quasielastic diffraction intensity, the low-energy region of RIXS spectra measured at the Cu L_3-edge was fitted with a sum of quasielastic, phonon, paramagnon, and background contributions as follows:

$$I^{Cu}_{RIXS}(E) = I^{Cu}_{el}(E) + I^{Cu}_{ph}(E) + I^{Cu}_{mag}(E) + I^{Cu}_{bg}(E) \quad (1)$$

Similarly for the O K-edge,

$$I^{O}_{RIXS}(E) = I^{O}_{el}(E) + I^{O}_{ph}(E) + I^{O}_{bg}(E) \quad (2)$$

Four terms on the right-hand side of Equation (1) represent a quasielastic, phonon, paramagnon, and background contribution on the RIXS intensity, respectively. The quasielastic peak and phonon excitation were described by Gaussian functions, whereas the paramagnon excitation was modeled by the response function of a damped harmonic oscillator multiplied with the Bose factor,[74] as follows:

$$I^{Cu,O}_{el}(E) = A_1 exp\left\{\frac{1}{2}\left(\frac{E - A_2}{A_3}\right)^2\right\} \quad (3)$$

$$I^{Cu,O}_{ph}(E) = \sum_{i=1}^{n} B_{3i-2} exp\left\{\frac{1}{2}\left(\frac{E - B_{3i-1}}{B_{3i}}\right)^2\right\} \quad (4)$$

$$I_{mag}^{Cu}(E) = C_1\left\{\frac{C_3 E}{(E^2 - C_2^2)^2 + E^2 C_3^2}\right\} \times \left\{\frac{1}{1 - e^{-E/C_4}}\right\} \quad (5)$$

$$I_{bg}^{Cu,O}(E) = D_1 E^2 + D_2 E + D_3 \quad (6)$$

An integer n indicates the number of phonon modes: $n = 1$ (only bond-stretching mode) for the Cu L_3-edge and $n = 2$ (bond-stretching and bond-buckling modes) for the O K-edge.[54] A_1, A_2, A_3, B_1, ⋯, B_n, and C_1, C_2, C_3 are the fitting parameters. C_4 was fixed to $k_B T$ with the measuring temperature T.

Angular-Dependent CDW Measurement: Angle- and momentum-dependent RIXS spectra across both H- and K-CDWs were obtained by taking advantage of the broad accessibility to in-plane rotation and the accurate control of sample manipulator. By controlling the polar angle θ, the azimuthal rotation angle ϕ, and the tilt angle χ using diffcalc, momentum-dependent RIXS scans could be obtained across the CDW peak with different scan angle α. Here, the scan angle α is defined as an angle between the scan direction and the longitudinal scan direction for each CDW. The representative scan directions are schematically described in the inset of Figure 1f,g. For Cu L_3-edge, the CDW peaks were measured in a range between -97.5° and 150°. For O K-edge, α was varied from 0° to 135°. Figures S2 and S3 (Supporting Information) present the momentum-dependence of integrated quasielastic intensity scans on H-CDW taken at different α as indicated. The momentum-dependence data was fitted with a combination of Gaussian functions, which represent a CDW peak, and a composite background.

$$I_{CDW}(Q) = G_1 exp\left\{\frac{1}{2}\left(\frac{Q - G_2}{G_3}\right)^2\right\} + G_5 exp\left(\frac{x - G_6}{G_7}\right) + G_8 Q^2 + G_9 Q + G_{10} \quad (7)$$

A full-width half-maximum (FWHM) of CDW peak was calculated by $2\sqrt{2\ln 2}G_3$ for each momentum-dependent profile. In Figures S2 and S3 (Supporting Information), the least-square fitted results are shown with solid lines at different scan angle α. The FWHMs of CDW peak are written in each panel. The angle-dependent FWHM shown in Figure 1h was fitted with an elliptical equation stated below:

$$FWHM(\alpha) = \frac{R_1 R_2}{\sqrt{\{b\cos(\alpha + \beta)\}^2 + \{b\sin(\alpha + \beta)\}^2}} \quad (8)$$

where R_1 (R_2) is the major (minor) axis of the ellipse and β is an offset angle. The grey-colored line presented in Figure 1h is the result of least square fitting, which gives $R_1 = 0.1184 \pm 0.0022$ r.l.u., $R_2 = 0.0656 \pm 0.0013$ r.l.u., and $\beta = 1.2 \pm 1.9°$. The offset angle $\beta \approx 0$ indicates that the CDW propagation is locked along two mutually-orthogonal Cu-O bond directions. For La-Bi2201 $x = 0.6$ (UD23K) samples, the data were obtained for three sample pieces from different batches.

Supporting Information

Supporting Information is available from the Wiley Online Library or from the author.

Acknowledgements

J.C. and J.L. contributed equally to this work. The authors thank Johan Chang, Stephen M. Hayden, Wei-Sheng Lee, Yayu Wang, and Qisi Wang for fruitful discussions. The authors also acknowledge Thomas Rice, the beamline technician at I21 beamline, for the technical supports. The authors thank Gavin Stenning and Daniel Nye for the Laue diffraction in the Materials Characterization Laboratory at the ISIS Neutron and Muon Source. This work was primarily supported by in-house research program of Diamond Light Source, Ltd. through beamtime proposals NT21277 and NT29623. J. C. acknowledges support from the National Research Foundation of Korea (NRF) grant funded by the Korean government (MSIT) through Sejong Science Fellowship (Grant No. RS-2023-00252768). J. L. acknowledges Diamond Light Source, Ltd. and Institute of Physics in Chinese Academy of Science for providing funding Grant 112111KYSB20170059 for the joint Doctoral Training under Contact STU0171. H. R. acknowledges funding and support from Engineering and Physical Sciences Research Council Centre for Doctoral Training through Grant EP/L015544/01 and EP/R0111141/1. H. D. acknowledges the financial support from the National Science Foundation of China (Grant 11888101), and the Ministry of Science and Technology of China (Grant 2016YFA0401000). S. J. acknowledges support from NSF under Grant DMR-1842056. J. P. acknowledges financial support by the SNSF Postdoc Mobility Project P400P2_180744.

Conflict of Interest

The authors declare no conflict of interest.

Data Availability Statement

The data that support the findings of this study are available from the corresponding author upon reasonable request.

Keywords

charge density wave, cuprates, quantum materials, resonant inelastic x-ray scattering, superconductivity, symmetry

Received: July 27, 2023
Revised: September 22, 2023
Published online: November 30, 2023

[1] B. Keimer, S. A. Kivelson, M. R. Norman, S. Uchida, J. Zaanen, *Nature* **2015**, *518*, 179.
[2] M. R. Norman, *Science* **2011**, *332*, 196.
[3] T. Timusk, B. Statt, *Rep. Prog. Phys.* **1999**, *62*, 61.
[4] C. M. Varma, *Phys. Rev. B* **2006**, *73*, 155113.
[5] D. L. Feng, D. H. Lu, K. M. Shen, C. Kim, H. Eisaki, A. Damascelli, R. Yoshizaki, J. i. Shimoyama, K. Kishio, G. D. Gu, S. Oh, A. Andrus, J. O'Donnell, J. N. Eckstein, Z. X. Shen, *Science* **2000**, *289*, 277.
[6] Y. He, Y. Yin, M. Zech, A. Soumyanarayanan, M. M. Yee, T. Williams, M. C. Boyer, K. Chatterjee, W. D. Wise, I. Zeljkovic, T. Kondo, T. Takeuchi, H. Ikuta, P. Mistark, R. S. Markiewicz, A. Bansil, S. Sachdev, E. W. Hudson, J. E. Hoffman, *Science* **2014**, *344*, 608.
[7] J. Zaanen, *SciPost Phys.* **2019**, *6*, 061.
[8] C. Yang, Y. Liu, Y. Wang, L. Feng, Q. He, J. Sun, Y. Tang, C. Wu, J. Xiong, W. Zhang, X. Lin, H. Yao, H. Liu, G. Fernandez, J. Xu, J. M. V. Jr, J. Wang, Y. Li, *Science* **2019**, *366*, 1505.
[9] C. Yang, H. Liu, Y. Liu, J. Wang, D. Qiu, S. Wang, Q. He, X. Li, P. Li, Y. Tang, J. Wang, X. C. Xie, J. M. V. Jr, J. Xiong, Y. Li, *Nature* **2021**, *601*, 205.
[10] V. Hinkov, D. Haug, B. Fauqué, Y. Sidis, A. Ivanov, C. Bernhard, C. T. Lin, B. Keimer, *Science* **2008**, *319*, 507.
[11] R. Daou, J. Chang, D. LeBoeuf, O. Cyr-Choiniére, F. Laliberté, N. Doiron-Leyraud, B. J. Ramshaw, R. Liang, D. A. Bonn, W. N. Hardy, L. Taillefer, *Nature* **2010**, *463*, 519.

[12] Y. Sato, S. Kasahara, H. Murayama, Y. Kasahara, E. G. Moon, T. Nishizaki, T. Loew, J. Porras, B. Keimer, T. Shibauchi, Y. Matsuda, *Nat. Phys.* **2017**, *13*, 1074.
[13] J. Wu, A. T. Bollinger, X. He, I. Bozovic, *Nature* **2017**, *547*, 432.
[14] J. M. Tranquada, B. J. Sternlieb, J. D. Axe, Y. Nakamura, S. Uchida, *Nature* **1995**, *375*, 561.
[15] J. M. Tranquada, J. D. Axe, N. Ichikawa, Y. Nakamura, S. Uchida, B. Nachumi, *Phys. Rev. B* **1996**, *54*, 7485.
[16] M. v. Zimmermann, A. Vigliante, T. Niemöller, N. Ichikawa, T. Frello, J. Madsen, P. Wochner, S. Uchida, N. H. Andersen, J. M. Tranquada, D. Gibbs, J. R. Schneider, *Europhys. Lett.* **1998**, *41*, 629.
[17] P. Abbamonte, A. Rusydi, S. Smadici, G. D. Gu, G. A. Sawatzky, D. L. Feng, *Nat. Phys.* **2005**, *1*, 155.
[18] J. E. Hoffman, E. W. Hudson, K. M. Lang, V. Madhavan, H. Eisaki, S. Uchida, J. C. Davis, *Science* **2002**, *295*, 466.
[19] H. Hanaguri, C. Lupien, Y. Kohsaka, D. H. Lee, M. Azuma, M. Takano, H. Takagi, J. C. Davis, *Nature* **2004**, *430*, 1001.
[20] G. Ghiringhelli, M. L. Tacon, M. Minola, S. Blanco-canosa, C. Mazzoli, N. B. Brookes, G. M. D. Luca, A. Frano, D. G. Hawthorn, F. He, T. Loew, M. M. Sala, D. C. Peets, M. Salluzzo, E. Schierle, R. Sutarto, G. A. Sawatzky, E. Weschke, B. Keimer, L. Braicovich, *Science* **2012**, *337*, 821.
[21] J. Chang, E. Blackburn, A. T. Holmes, N. B. Christensen, J. Larsen, J. Mesot, R. Liang, D. A. Bonn, W. N. Hardy, A. Watenphul, M. v. Zimmermann, E. M. Forgan, S. M. Hayden, *Nat. Phys.* **2012**, *8*, 871.
[22] M. Fujita, H. Goka, K. Yamada, M. Matsuda, *Phys. Rev. Lett.* **2002**, *88*, 167008.
[23] T. Wu, H. Mayaffre, S. Krämer, M. Horvatić, C. Berthier, W. N. Hardy, R. Liang, D. A. Bonn, M. Julien, *Nature* **2011**, *477*, 191.
[24] C. Howald, H. Eisaki, N. Kaneko, A. Kapitulnik, *Proc. Natl. Acad. Sci. U. S. A.* **2003**, *100*, 9705.
[25] W. D. Wise, M. C. Boyer, K. Chatterjee, T. Kondo, H. Ikuta, Y. Wang, E. W. Hudson, *Nat. Phys.* **2008**, *4*, 696.
[26] M. Vershinin, S. Misra, S. Ono, Y. Abe, Y. Ando, A. Yazdani, *Science* **2004**, *303*, 1995.
[27] E. H. da Silva Neto, P. Aynajian, A. Frano, R. Comin, E. Schierle, E. Weschke, A. Gyenis, J. Wen, J. Schneeloch, z. Xu, S. Ono, G. Gu, M. L. Tacon, A. Yazdani, *Science* **2014**, *343*, 393.
[28] P. Cai, W. Ruan, Y. Y. Peng, C. Ye, X. Li, Z. Hao, X. Zhou, D. H. Lee, Y. Wang, *Nat. Phys.* **2016**, *12*, 1047.
[29] X. Li, C. Zhou, Y. Ding, H. Yan, S. Ye, H. Li, Z. Hao, L. Zhao, X. Zhou, Y. Wang, *Phys. Rev. X* **2021**, *11*, 011007.
[30] R. Comin, A. Frano, M. M. Yee, Y. Yoshida, H. Eisaki, E. Schierle, E. Weschke, R. Sutarto, F. He, A. Soumyanarayanan, Y. He, M. L. Tacon, I. S. Elfimov, J. E. Hoffman, G. A. Sawatzky, B. Keimer, A. Damascelli, *Science* **2014**, *343*, 390.
[31] E. H. da Silva Neto, R. Comin, F. He, R. Sutarto, Y. Jiang, R. L. Greene, G. A. Sawatzky, A. Damascelli, *Science* **2015**, *347*, 282.
[32] E. H. da Silva Neto, B. Yu, M. Minola, R. Sutarto, E. Schierle, F. Boschini, M. Zonno, M. Bluschke, J. Higgins, Y. Li, G. Yu, E. Weschke, F. He, M. L. Tacon, R. L. Greene, M. Greven, G. A. Sawatzky, B. Keimer, A. Damascelli, *Sci. Adv.* **2016**, *2*, e1600782.
[33] R. Comin, A. Damascelli, *Ann. Rev. Condens. Matter Phys.* **2016**, *7*, 369.
[34] R. Comin, R. Sutarto, E. H. da Silva Neto, L. Chauviere, R. Liang, W. N. Hardy, D. A. Bonn, F. He, G. A. Sawatzky, A. Damascelli, *Science* **2015**, *347*, 1335.
[35] R. Comin, R. Sutarto, F. He, E. H. da Silva Neto, L. Chauviere, A. Frano, R. Liang, W. N. Hardy, D. A. Bonn, Y. Yoshida, H. Eisaki, A. J. Achkar, D. G. Hawthorn, B. Keimer, G. A. Sawatsky, A. Damascelli, *Nature Materials* **2015**, *14*, 796.
[36] J. Choi, Q. Wang, S. Jöhr, N. B. Christensen, J. Küspert, D. Bucher, D. Biscette, M. H. Fischer, M. Hücker, T. Kurosawa, N. Momono, M. Oda, O. Ivashko, M. von Zimmermann, M. Janoschek, J. Chang, *Phys. Rev. Lett.* **2022**, *128*, 207002.
[37] G. Simutis, J. Küspert, Q. Wang, J. Choi, D. Bucher, M. Boehm, F. Bouradot, M. Bertelsen, C. N. Wang, T. Kurosawa, N. Momono, M. Oda, M. Månnson, Y. Sassa, M. Janoschek, N. B. Christensen, J. Chang, D. G. Mazzone, *Commun. Phys.* **2022**, *5*, 296.
[38] H. H. Kim, S. M. Souliou, M. E. Barber, E. Lefrancois, M. Minola, M. Tortora, R. Heid, N. Nandi, R. A. Borzi, G. Garbarino, A. Bosak, J. Porras, T. Loew, M. König, P. M. Moll, A. P. Mackenzie, B. Keimer, C. W. Hicks, M. L. Tacon, *Science* **2018**, *362*, 1040.
[39] H. H. Kim, E. Lefrancois, K. Kummer, R. Fumagalli, N. B. Brookes, D. Betto, S. Nakata, M. Tortora, J. Porras, T. Loew, M. E. Barber, L. Braicovich, A. P. Mackenzie, C. W. Hicks, B. Keimer, M. Minola, M. L. Tacon, *Phys. Rev. Lett.* **2021**, *126*, 037002.
[40] Y. Kohsaka, C. Taylor, K. Fujita, A. Schmidt, C. Lupien, T. Hanaguri, M. Azuma, M. Takano, H. Eisaki, H. Takagi, S. Uchida, J. C. Davis, *Science* **2007**, *315*, 1380.
[41] M. J. Lawler, K. Fujita, J. Lee, A. R. Schmidt, Y. Kohsaka, C. K. Kim, H. Eisaki, S. Uchida, J. C. Davis, J. P. Sethna, E. A. Kim, *Nature* **2010**, *466*, 347.
[42] Y. Kohsaka, T. Hanaguri, M. Azuma, M. Takano, J. C. Davis, H. Takagi, *Nat. Phys.* **2012**, *8*, 534.
[43] K. Fujita, M. H. Hamidian, S. D. Edkins, C. K. Kim, Y. Kohsaka, M. Azuma, M. Takano, H. Takagi, H. Eisaki, S. Uchida, A. Allais, M. J. Lawler, E. A. Kim, S. Sachdev, J. C. S. Davis, *Proc. Natl. Acad. Sci. USA* **2014**, *111*, E3026.
[44] M. H. Hamidian, S. D. Edkins, C. K. Kim, J. C. Davis, A. P. Mackenzie, H. Eisaki, S. Uchida, M. J. Lawler, E. A. Kim, S. Sachdev, K. Fujita, *Nat. Phys.* **2016**, *12*, 150.
[45] S. Kivelson, E. Fradkin, V. Emery, *Nature* **1998**, *393*, 550.
[46] S. A. Kivelson, I. P. Bindloss, E. Fradkin, V. Oganesyan, J. M. Tranquada, A. Kapitulnik, C. Howald, *Rev. Mod. Phys.* **2003**, *75*, 1201.
[47] V. Cvetkovic, Z. Nussinov, S. Mukhin, J. Zaanen, *Europhys. Lett.* **2008**, *81*, 27001.
[48] E. A. Huang, C. B. Mendl, S. Liu, S. Johnston, H. C. Jiang, B. Moritz, T. P. Devereaux, *Science* **2017**, *358*, 1161.
[49] P. Mai, S. Karakuzu, G. Balduzzi, S. Johnston, T. A. Maier, *Proc. Natl. Acad. Soc. USA* **2022**, *119*, e2112806119.
[50] E. Fradkin, S. A. Kivelson, M. J. Lawler, J. P. Eisenstein, A. P. Mackenzie, *Ann. Rev. Condens. Matter Phys.* **2010**, *1*, 153.
[51] D. F. Agterberg, J. C. S. Davis, S. D. Edkins, E. Fradkin, D. J. V. Harlingen, S. A. Kivelson, P. A. Lee, L. Radzihovsky, J. M. Tranquada, Y. Wang, *Ann. Rev. Condens. Matter Phys.* **2020**, *11*, 231.
[52] Y. Y. Peng, M. Salluzzo, X. Sun, A. Ponti, D. Betto, A. M. Ferretti, F. Fumagalli, K. Kummer, M. L. Tacon, X. J. Zhou, N. B. Brookes, L. Braicovich, G. Ghiringhelli, *Phys. Rev. B* **2016**, *94*, 184511.
[53] Y. Y. Peng, R. Fumagalli, Y. Ding, M. Minola, S. Caprara, D. Betto, M. Bluschke, G. M. D. Luca, K. Kummer, E. Lefrancois, M. Salluzzo, H. Suzuki, M. L. Tacon, X. J. Zhou, N. B. Brookes, B. Keimer, L. Braicovich, M. Grilli, G. Ghiringhelli, *Nat. Mater.* **2018**, *17*, 697.
[54] J. Li, A. Nag, J. Pelliciari, H. Robarts, A. Walters, M. Garcia-Fernandez, H. Eisaki, D. Song, H. Ding, S. Johnston, R. Comin, K. J. Zhou, *Proc. Natl. Acad. Acad. USA* **2020**, *117*, 16219.
[55] W. S. Lee, K. J. Zhou, M. Hepting, J. Li, A. Nag, A. C. Walters, M. Garcia-Fernandez, H. C. Robarts, M. Hashimoto, H. Lu, B. Nosarzewski, D. Song, H. Eisaki, Z. X. Shen, B. Moritz, J. Zaanen, T. P. Devereaux, *Nat. Phys.* **2021**, *17*, 53.
[56] B. V. Fine, *Science* **2016**, *351*, 235a.
[57] J. A. Robertson, S. A. Kivelson, E. Fradkin, A. C. Fang, A. Kapitulnik, *Phys. Rev. B* **2006**, *74*, 134507.
[58] H. Li, H. Li, Z. Wang, S. Wan, H. Yang, H. H. Wen, *npj Quantum Mater.* **2023**, *8*, 18.
[59] Z. Du, H. Li, G. Gu, A. N. Pasupathy, J. M. Tranquada, K. Fujita, *Phys. Rev. X* **2023**, *13*, 021025.

[60] V. Thampy, S. Blanco-Canosa, M. García-Fernández, M. P. M. Dean, G. D. Gu, M. Först, T. Loew, B. Keimer, M. L. Tacon, S. B. Wilkins, J. P. Hill, *Phys. Rev. B* **2013**, *88*, 024505.
[61] V. Thampy, M. P. M. Dean, N. B. Christensen, L. Steinke, Z. Islam, M. Oda, M. Ido, N. Momono, S. B. Wilkins, J. P. Hill, *Phys. Rev. B* **2014**, *90*, 100510(R).
[62] Q. Wang, M. Horio, K. von Arx, Y. Shen, D. J. Mukkattukavli, Y. Sassa, O. Ivashko, C. E. Matt, S. Pyon, T. Takayama, H. Takagi, T. Kurosawa, N. Momono, M. Oda, T. Adachi, S. M. Haidar, Y. Koike, Y. Tseng, W. Zhang, J. Zhao, K. Kummer, M. Garcia-Fernandez, K. J. Zhou, N. B. Christensen, H. M. Rønnow, T. Schmitt, J. Chang, *Phys. Rev. Lett.* **2020**, *124*, 187002.
[63] Q. Wang, K. von Arx, D. G. Mazzone, S. Mustafi, M. Horio, J. Küspert, J. Choi, D. Bucher, W. Zhang, T. C. Asmara, Y. Sassa, M. Månsson, N. B. Christensen, M. Janoscheck, T. Kurosawa, N. Momono, M. Oda, M. H. Fischer, T. Schmitt, J. Chang, *Nature Communications* **2022**, *13*, 1795.
[64] G. Campi, A. Bianconi, N. Poccia, G. Bianconi, L. Barba, G. Arrighetti, D. Innocenti, J. Karpinski, N. D. Zhigadlo, S. M. Kazakov, M. Burghammer, M. v. Zimmermann, M. Sprung, A. Ricci, *Nature* **2015**, *525*, 359.
[65] J. J. Wen, H. Huang, S. J. Lee, H. Jang, J. Knight, Y. S. Lee, M. Fujita, K. M. Suzuki, S. Asano, S. A. Kivelson, C. C. Kao, J. S. Lee, *Nat. Commun.* **2019**, *10*, 3269.
[66] J. Chang, E. Blackburn, O. Ivashko, A. T. Holmes, N. B. Christensen, M. Hücker, R. Liang, D. A. Bonn, W. N. Hardy, U. Rütt, M. v. Zimmermann, E. M. Forgan, S. M. Hayden, *Nat. Commun.* **2016**, *7*, 11494.
[67] J. Choi, O. Ivashiko, E. Blackburn, R. Liang, D. A. Bonn, W. N. Hardy, A. T. Holmes, N. B. Christensen, M. Hücker, S. Gerber, O. Gutowski, U. Rütt, M. v. Zimmermann, E. M. Forgan, S. M. Hayden, J. Chang, *Nat. Commun.* **2020**, *11*, 990.
[68] Q. Li, M. Hucker, G. D. Gu, A. M. Tsvelik, J. M. Tranquada, *Phys. Rev. Lett.* **2007**, *99*, 067001.
[69] E. Berg, E. Fradkin, E. A. Kim, S. A. Kivelson, V. Oganesyan, J. M. Tranquada, S. C. Zhang, *Phys. Rev. Lett.* **2007**, *99*, 127003.
[70] Z. Du, H. Li, S. H. Joo, E. P. Donoway, J. Lee, J. C. S. Davis, G. Gu, P. D. Johnson, K. Fujita, *Nature* **2020**, *580*, 65.
[71] S. Ye, C. Zhou, H. Yan, Y. Ji, M. Xu, Z. Dong, Y. Chen, X. Zhou, Y. Wang, *Nat. Phys.* **2023**, *19*, 1301.
[72] H. Lu, P. Cheng, L. Fang, H. H. Wen, *Supercond. Sci. Technol.* **2008**, *21*, 125024.
[73] K. J. Zhou, A. Walters, M. Garcia-Fernandez, T. Rice, M. Hand, A. Nag, J. Li, S. Agrestini, P. Garland, H. Wang, S. Alcock, I. Nistea, B. Nutter, N. Rubies, G. Knap, M. Gaughran, F. Yuan, P. Chang, J. Emmins, G. Howell, *J. Synchrotron Rad.* **2022**, *29*, 1.
[74] C. Monney, T. Schmitt, C. E. Matt, J. Mesot, V. N. Strocov, O. J. Lipscombe, S. M. Hayden, J. Chang, *Phys. Rev. B* **2016**, *93*, 075103.